Microporous and Mesoporous Materials 167 (2013) 188–197

Contents lists available at SciVerse ScienceDirect

Microporous and Mesoporous Materials

journal homepage: www.elsevier.com/locate/micromeso

Analytical representation of micropores for predicting gas adsorption in porous materials

Aaron W. Thornton [a,*], Scott A. Furman [a], Kate M. Nairn [a], Anita J. Hill [a], James M. Hill [b], Matthew R. Hill [a,c]

[a] CSIRO Materials Science and Engineering, Locked Bag 33, Clayton Sth MDC, Vic 3169, Australia
[b] Nanomechanics Group, School of Mathematical Sciences, The University of Adelaide, SA 5005, Australia
[c] School of Chemistry, University of Melbourne, Vic 3010, Australia

ARTICLE INFO

Article history:
Received 10 November 2011
Received in revised form 3 August 2012
Accepted 3 September 2012
Available online 12 September 2012

Keywords:
Adsorption
Metal–organic framework
Nanotube
Activated carbon
Potential energy

ABSTRACT

A straightforward method for the prediction of the gas storage capabilities of porous materials has been established. The Topologically Integrated Mathematical Thermodynamic Adsorption Model (TIMTAM) combines analytical surface potential energies with classical physisorption thermodynamics in a computationally inexpensive fashion. Experimental and simulated isotherms from leading sorbent candidates such as metal–organic frameworks (MOFs), zeolitic imidazolate frameworks (ZIFs), carbon nanotubes and activated carbons have been used to verify the model. Furthermore, the effect of pore size and shape upon gas storage characteristics is explored using the TIMTAM routine.

1. Introduction

One of the challenges of the 21st century is the generation, storage and delivery of energy in an affordable, renewable and clean fashion [1,2]. The ability to efficiently capture, store and release gases plays an important role in addressing such issues, for example: carbon capture and storage (CCS) for clean coal, petroleum and natural gas combustion [3–5]; methane capture and storage for climate control or safe energy transport [6,7], and hydrogen capture and storage from photolytic water splitting or coal gasification for clean combustion or fuel cell technologies [1]. Porous materials are poised to meet such challenges.

The leading candidates for efficient high capacity gas storage porous materials are metal–organic frameworks (MOFs) [8–11], zeolitic imidazolate frameworks (ZIFs) [12–14], nanotubes [15–17], and graphenic carbons [18–22], which can each undergo physisorption, with capacity closely related to surface area. The usage of such adsorbents depends strongly on key factors such as the capacity, operating temperature, cyclability and kinetics of operation. Within a porous gas adsorbent, the nature of the pores is integral to addressing these issues, with pore shape, size, concentration and surface chemistry all important to the overall performance.

Experimental materials discovery has led to substantial improvements in gas storage performance. However, the formulation of improved guidelines for further development of new materials could greatly speed this process. Whilst detailed, atomic level resolution modeling can elucidate the fundamental atomic interactions, a model that focuses on the overall impact of pore topology on overall performance is pertinent. Furthermore, a quick, accurate, yet accessible model would strengthen the feedback loop between experimentalists and modelers.

Modeling techniques for addressing physisorption range in complexity, accuracy and utility. Firstly there are fundamental equations such as the Langmuir single-layer model [23] and the Brunauer, Emmett and Teller (BET) multi-layer model [24] that have simplicity, such that anyone can calculate adsorption properties without the need for extensive computational or modeling expertise. Then, on a more complex level, there are the simulation (or computational) techniques such as Molecular Dynamics (MD) [25–30], Monte Carlo (MC) [16,30–34] and those based on ab initio principles [35–41] or mean-field density functional theories [42,43]. Each of these techniques offer useful functions that have significant impact on the field of materials science and more specifically on the current demand for high performing membranes and adsorbents [44]. The simple equations offer quick estimates of surface area and heat of adsorption from experimental adsorption isotherms, while the computationally-expensive simulation techniques offer in-depth detail and prediction of all aspects of adsorption within specific atomic structures. A tool that is missing

* Corresponding author. Tel.: +61 3 9545 8018; fax: +61 3 9545 2837.
E-mail address: aaron.thornton@csiro.au (A.W. Thornton).

1387-1811/$ - see front matter © 2012 Elsevier Inc. All rights reserved.
http://dx.doi.org/10.1016/j.micromeso.2012.09.002

for the porous materials community is a simple predictive model that can speedily estimate gas uptakes based on obtainable details such as pore size, shape and composition. Therefore we present a technique that exists on the middle ground – it is as straightforward as the BET type models and as predictive as the simulation techniques. As such it can be readily applied by those without extensive modeling experience. We envisage that this technique will also be utilized for computational screening of large databases of potential adsorbents where detailed simulation techniques are not suitable.

By exploiting thermodynamic and kinetic principles we develop a model that can be used to investigate the gas adsorption phenomenon and which encompasses the main characteristics found by statistical simulation studies. Essential input factors for the model include temperature, pressure, and pore geometry (which is used to derive the potential energy landscape, free volume and surface area). For complex atomic structures, algorithms for calculating potential energy, free volume and surface area are readily available [45–48]. For structures with simple pore geometries that can be approximated by spheres, cylinders or slits, we provide analytical formulations which are used throughout this study. These formulations are ideal as they do not rely on specific atom positions for which computationally expensive methods are needed to calculate the potential energy at each point within the structure. Therefore, by approximating the topology, integrating the potential energy within the cavity and incorporating thermodynamic theory we establish the Topologically Integrated Mathematical Thermodynamic Adsorption Model (TIMTAM). The major advantage of our TIMTAM approach is that it provides researchers with analytical formulae that are computationally instantaneous, and therefore many distinct scenarios can be rapidly investigated to accelerate material design [11]. The primary function of the model will be the simulation of adsorption isotherms from estimates of pore volume, size and shape.

The following section outlines the basic theory and formulations for the model. Experimental and simulation results are then used to validate the model, followed by an investigation into the effect that pore shapes have on adsorption. This approach has already been used to investigate the performance of a new class of adsorbents, MOFs impregnated with nanostructures [11]. The model successfully described the uptake within existing MOFs and predicted an enhanced hydrogen and methane uptake within MOFs infused with fullerenes and decorated fullerenes. Here we fully present the model in its complete form, demonstrating its ability to model gas uptake in a range of adsorbents such as MOFs, ZIFs, nanotubes and activated carbons, and direct the reader to a graphical user interface, Adsorb IT, that we have developed to demonstrate the speed, versatility, usability and accuracy of the TIMTAM approach.

2. Theory and mathematical formulation

The interactions between a gas molecule and a surface, arising from van der Waals forces, are well described by the Lennard-Jones (L-J) potential energy function. This potential is known in this context as the potential energy for adsorption, found by integrating the atom–atom L-J function over the surface. Here we assume a continuous surface and formulate the potential energy within cavities that can be represented as analytical geometric shapes. For conventional Monte Carlo algorithms, the potential energy is calculated numerically where the surface is treated as discrete atoms to produce a potential map [45,47,48]. However, since generating the potential map is the most time-consuming element of a Monte-Carlo algorithm, it is advantageous to approximate the geometry where possible. Here the available analytical formulations for the potential energy within three different cavity shapes are given below and we refer the reader to [49,50] for further details.

Slit-shaped cavity:

$$PE_{\text{slit}}(\rho) = \eta(-AH_{\text{slit}}[4] + BH_{\text{slit}}[10]),$$
$$H_{\text{slit}}[n] = \frac{2\pi}{n}\left(\frac{1}{((d/2)-\rho)^n} + \frac{1}{((d/2)+\rho)^n}\right) \quad (1)$$

Cylindrical cavity:

$$PE_{\text{cyl}}(\rho) = \eta(-AH_{\text{cyl}}[3] + BH_{\text{cyl}}[6]),$$
$$H_{\text{cyl}}[n] = \frac{2\pi^2 d^2}{(d)^{2n}(2n-2)!}\sum_{j=0}^{\infty}\left(\frac{\rho^j(2n+2j-2)!}{(2d)^j j!(n+j-1)!}\right)^2 \quad (2)$$

Spherical cavity:

$$PE_{\text{sph}}(\rho) = \eta(-AH_{\text{sph}}[6] + BH_{\text{sph}}[12]),$$
$$H_{\text{sph}}[n] = \frac{\pi d}{\rho(2-n)}\left(\frac{1}{(\rho+(d/2))^{n-2}} - \frac{1}{(\rho-(d/2))^{n-2}}\right) \quad (3)$$

ρ is the distance of the gas molecule from the cavity center, d represents the cavity dimension (distance between surface nuclei) and η is the atomic surface density of the cavity wall. A and B are the attractive and repulsive constants, respectively, defined as $A = 4\varepsilon\sigma^6$ and $B = 4\varepsilon\sigma^{12}$ (σ is the kinetic diameter and ε is the well depth for interacting pairs of atoms). Potential energy maps are shown within each cavity shape in Fig. 1. The potential minimum is deepest within cavities with higher curvature where the gas is closer to more surface atoms. Note that this potential is independent of both temperature and pressure. The kinetic energy of the gas, as a result of the specified temperature, relative to the size of the potential energy for adsorption, determines the probability that surface adsorption of a gas molecule will occur [51].

According to kinetic theory, the average translational kinetic energy per molecule KE_{gas} in an ideal gas is equal to $3k_BT/2$ where k_B is the Boltzmann constant and T is the temperature. Usually the values for the kinetic energy of a gas molecule KE_{gas} and the potential energy for adsorption PE_{surface} are similar and hence there exists a continuous mixture of adsorbed and bulk phases rather than the discrete monolayer adsorption as assumed by the Langmuir treatment [23]. Generally speaking, if $KE_{\text{gas}} < PE_{\text{surface}}$ then surface adsorption occurs. Following this, the probability of adsorption at a distance ρ from the cavity center can be approximated as

$$P_{\text{ad}}(\rho) = 1 - \exp\left(\frac{-|PE(\rho)|}{KE_{\text{gas}}}\right), \quad (4)$$

where $\exp(-|PE|/KE_{\text{gas}})$ is the probability that $KE_{\text{gas}} > PE_{\text{surface}}$, i.e. the probability that a gas molecule is in the bulk phase. Note this criterion is of similar form to the acceptance probability used in MC simulations, though in this case we are not calculating the acceptance of a certain particle but rather determining the phase likely to exist at this position.

The total free volume V_f within a cavity is defined here as the volume for which the potential energy is less than zero. In other words, the boundaries for this free volume are located where the potential energy for adsorption is zero at a distance ρ_0 from the center of the cavity, indicated in Fig. 1. Alternatively, temperature dependent boundaries could be chosen at which the potential energy is equal to the average kinetic energy, which gives a more accurate free volume but is found not to significantly affect the total uptake. Here the former definition is used. By integrating the probability function in Eq. (4) over the total free volume we determine the volume free for adsorption V_{ad} as follows,

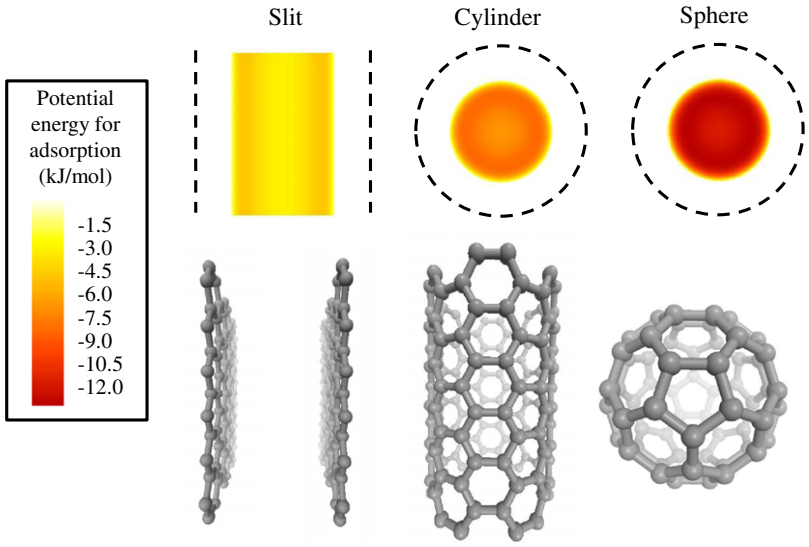

Fig. 1. Analytical representations for microcavities found in adsorbent materials. Potential energy maps for adsorption within slit-shaped, cylindrical and spherical cavities. Values are calculated by assuming carbon surfaces at an atomic dimension d of 30 Å.

$$V_{ad} = \int_{V_f} P_{ad}(\rho) d\rho, \tag{5}$$

and similarly, the volume free for bulk gas is calculated as

$$V_{bulk} = \int_{V_f} [1 - P_{ad}(\rho)] d\rho \tag{6}$$

See Supplementary information for expanded integrals. This partition of free volume offers a convenient framework for treating the system as two phases in equilibrium. The final step in the model is to calculate the actual number of gas molecules within the total free volume (or in each phase) at a certain temperature and pressure. Equations of states are commonly used for this purpose [52–54]. The ideal gas law is a thermodynamically consistent equation that assumes no interaction between molecules (i.e. no potential energy). Hence the total internal energy from kinetic energy only is as follows, $pV = 2NK_{gas}N_A/3 = NRT$, where N is the number of molecules, p is the pressure, N_A is Avogadro's Number and R is the universal gas constant. This equation of state is appropriate to govern our bulk gas phase apart from the assumption that each molecule is a point mass with no occupied volume which will provide inaccurate results for situations involving small pores, high pressures and low temperatures. Therefore we use the modified van der Waals equation of state accordingly,

$$p(V_{bulk}/n_{bulk} - v_0) = RT \tag{7}$$

where $n_{bulk} \times N_A$ is the number of molecules in the bulk gas phase and v_0 is the occupied volume of closely packed gas molecules.

An appropriate equation of state for the adsorbed phase does not exist, to the best of our knowledge, apart from the virial equation, which has no explicit predictive power [55]. Here we establish an equation of state which is of a similar form to the Dieterici equation of state [53,56], and that satisfies the following criteria: (1) when potential energy equals zero, the equation of state reduces to the ideal gas law and (2) when the potential energy tends towards negative infinity the equation of state represents a solid phase. Hence we propose the following,

$$p(V_{ad}/n_{ad} - v_0) = \alpha RT \exp(-|PE^*|/RT), \tag{8}$$

with PE^* defined as follows,

$$PE^* = \omega PE_{min} + (1 - \omega) PE_{cent}, \tag{9}$$

where $n_{ad} \times N_A$ is the number of molecules in the adsorbed phase, ω represents the weighted contribution of the potential minimum PE_{min} and the potential at the center PE_{cent} of the cavity, and α is the proportionality constant such that αRT (or $\alpha k_B T$) is a measure of the kinetic energy per mole (or molecule) in the adsorbed phase due to the translational movement of the adsorbed molecules parallel to the cavity surface. Keep in mind that the kinetic energy per molecule restricted to one dimension is $k_B T/2$, two dimensions is $k_B T$, and three dimensions is $3k_B T/2$. Hence, smaller α translates to more restricted motion and consequently more heat loss upon adsorption.

To demonstrate the relationship between this formulation and the equations used in Grand Canonical Monte Carlo (GCMC) simulations, we calculate the heat of adsorption $\bar{h}$ through the thermodynamic equation [55,57],

$$\bar{h} = R\left[\frac{\partial \ln p}{\partial(1/T)}\right]_n \tag{10}$$

By rearranging Eq. (8) to make p a function of T and then integrating we determine the isosteric heat of adsorption (see Supplementary information),

$$\bar{h}_{st} = |PE^*| + RT, \tag{11}$$

which is identical to that used in GCMC simulations [32,58]. Additionally, a reasonable approximation of the heat of adsorption is given by Everett and Powl [59] as $\bar{h} = |PE_{min}| + \alpha_1 RT$, where $\alpha_1 = 0.5$ due to parallel motion across the surface and vibration normal to the surface. Therefore the TIMTAM construction has kinetic and thermodynamic consistency, which allows comparison with approaches based on both statistical and analytical arguments.

Note that n_{ad} is not to be confused with the excess amount N_{ex} used frequently in the literature [60]. N_{ex} is defined as the amount of molecules in excess of the theoretical amount of molecules that the cavity would contain in the bulk gas phase. While $n_{ad} \times N_A$ is the actual amount of molecules in adsorbed phase, assuming a partitioning of free volume as defined previously (Eqs. 5 and 6).

Finally, the total amount of moles are found ($n = n_{ad} + n_{bulk}$) and the gravimetric uptake is calculated in the following way,

$$\text{wt.}\% = \frac{nm}{(nm + M)} \times 100, \tag{12}$$

where m is the mass of a gas molecule and M is the mass of the cavity wall. In addition, the volumetric uptake is calculated as

$$\bar{v} = \frac{nm}{V}, \tag{13}$$

where V is the total volume of the cavity including the free volume and occupied volume.

To summarize, the structure topology is approximated with continuous surfaces with analytical potential energy formulations for adsorption which are then used to determine the temperature-dependent probability of adsorption throughout the cavity. By integrating the probability of adsorption over the free volume, the volume free for adsorption is found and in the same way the volume free for bulk phase is also found. Finally, temperature and pressure dependent equations of states are used to determine the quantity of gas molecules in each phase within the cavity (See Supplementary information for density profile predictions that further demonstrate the TIMTAM construct).

For general users of the model, the following step-by-step instructions are given:

(1) Define pore shape, pore size and pore surface composition (e.g. cylindrical pore with diameter of 15 Å and 0.4 carbon atoms per Å^2 of surface).
(2) Calculate potential energy using Eqs. (1, 2 or 3).
(3) Choose temperature and calculate the probability of adsorption using Eq. (4).
(4) Calculate amount of volume for gas phase and amount of volume for adsorbed phase using Eqs. (5 and 6).
(5) Choose pressure and calculate total uptake using Eqs. (7 and 8).

3. Results and discussion

To demonstrate the capability of TIMTAM to accurately predict adsorption performance within a range of porous adsorbents we reproduce the results found from MC simulations for hydrogen uptake within carbon slits and carbon nanotubes by Rzepka et al. [54], experimental results for methane uptake in carbon slits from Aukett et al. [61], MC simulations for hydrogen uptake within MOFs by Ryan et al. [62], experimental results for hydrogen uptake within MOFs from Kaye et al. [63], and experimental and simulation results for carbon dioxide within ZIFs from Perez-Pellitero et al. [64] All calculations were carried out using Maple software [65]. The Maple code has been translated to Fortran and incorporated into a graphical user interface, Adsorb IT, which is available upon request [66].

Comparison with existing simulation results is a good test of the model since all the variables are known, as opposed to experimental results where some variables can be difficult to control accurately. Rzepka et al. [54] have simulated the gravimetric and volumetric hydrogen uptake in carbon slits and carbon nanotubes of various sizes d at a range of pressures and temperatures. Here we represent the slits and nanotubes analytically according to Eqs. (1 and 2), respectively, and use the same L-J parameters as Rzepka et al. listed in Table 1. Figs. 2 and 3 show excellent fits of the model to the simulation results for gravimetric and volumetric uptakes for slits and nanotubes. Despite its simplicity, it is clear that the model captures the essential characteristics of the simulation results.

Rzepka et al. [54] noted that the small peaks in the uptake correspond to pores into which only an individual hydrogen molecule can fit. Since our model utilizes a continuum perspective it is difficult to mimic the uptake of an individual molecule accurately. However, the pore size for this situation is very close to the pore size in which the potential is at a minimum and therefore the model is capable of mimicking the peak uptake especially within the slit-shaped cavities, see Fig. 2.

Recently, Herrera et al. [69] developed and implemented a mass balance (MB) method that predicted the pore size distribution of activated carbon AX-21 that can roughly be described as a bimodal distribution centered around 12 and 21 Å. The model also reproduced the experimental methane uptake within this material. A comparison of TIMTAM and Aukett's results are shown in Fig. 4. An excellent fit is observed and the parameter values are listed in Table 1.

Since the leading candidate hydrogen storage materials are MOFs it is important that the model is capable of describing their uptake performance, as shown in Fig. 5. Here we consider the isoreticular MOF-5 (a.k.a. IRMOF-1) [8] with cubic periodicity which is approximated here by a cubic array of spherical cavities. The framework atoms zinc, oxygen, carbon and hydrogen, denoted by the subscripts $i = 1, 2, 3$ and 4, are assumed to be distributed on the surface of the continuum spherical cavity at diameter d. Therefore the potential energy for adsorption within the cavity can be estimated as,

$$PE_{MOF}(\rho) = \sum_{i=1}^{4} PE_{\mathrm{sph,\,i}}(\rho), \tag{14}$$

where the parameters in Eq. (3) are given by $\eta = \sum \eta_i$, $A = \sum A_i$ and $B = \sum B_i$. The L-J parameter values are taken from the Dreiding force field calculations [67] and are listed in Table 1 along with all the other parameter values used in the model. The spherical cavity size d was set to 21.8 Å such that the amount of free volume matched that found by simulation, see Supplementary information for more details. Despite the geometrical approximation, the TIMTAM results agree well with the simulation and experimental results.

Table 1
Parameter values used for TIMTAM predictions. ω and α were fitted per family of structures. Additionally, the occupied volume of compressed hydrogen $v_0 = 0.0156$ L/mol, methane $v_0 = 0.043$ L/mol and carbon dioxide $v_0 = 0.036$ L/mol (calculated from critical parameters).

Data from literature	Gas-adsorbent	Kinetic diameter σ (Å)	Well depth ε/k_B (K)	Surface density η (No./Å^2)	ω	α
Hydrogen uptake carbon nanotubes and carbon slits Rzepka et al. [54]	H_2–C:	3.19	30.5	0.382	0.80	1.17
Methane uptake carbon slits Aukett et al. [61]	CH_4–C:	3.64	84.19	0.382	0.55	1.24
Carbon dioxide uptake ZIFs Perez-Pellitero et al. [64]	CO_2–C:	3.41	84.35	See Supplementary information	1	0.55
	CO_2–H:	2.87	54.60			
	CO_2–N:	3.20	68.37			
	CO_2–Cl:	3.41	124.02			
	CO_2–Zn:	2.82	91.66			
Hydrogen uptake IRMOF-1 Kaye et al. [63]	H_2–C:	3.22	41.90	0.064	1	0.41
	H_2–O:	3.00	42.05	0.070		
	H_2–H:	2.91	16.76	0.032		
	H_2–Zn:	3.50	31.89	0.021		

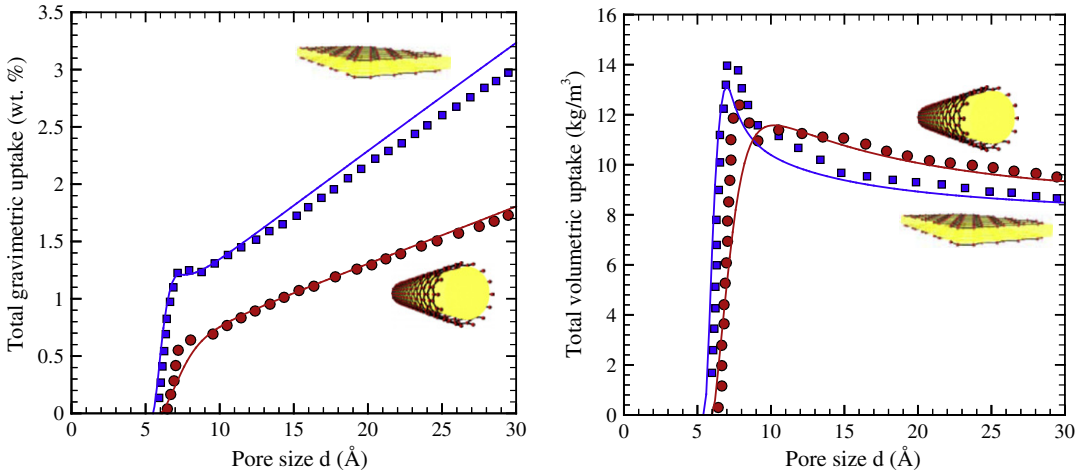

Fig. 2. TIMTAM prediction (solid lines) compared to simulation results for hydrogen gravimetric (left) and volumetric (right) uptakes within carbon slits (blue squares) and carbon nanotubes (red circles) of different pore size *d* at 300 K and 98.7 atm. Simulation data from Rzepka et al. [54]. (For interpretation of the references to color in this figure legend, the reader is referred to the web version of this article.)

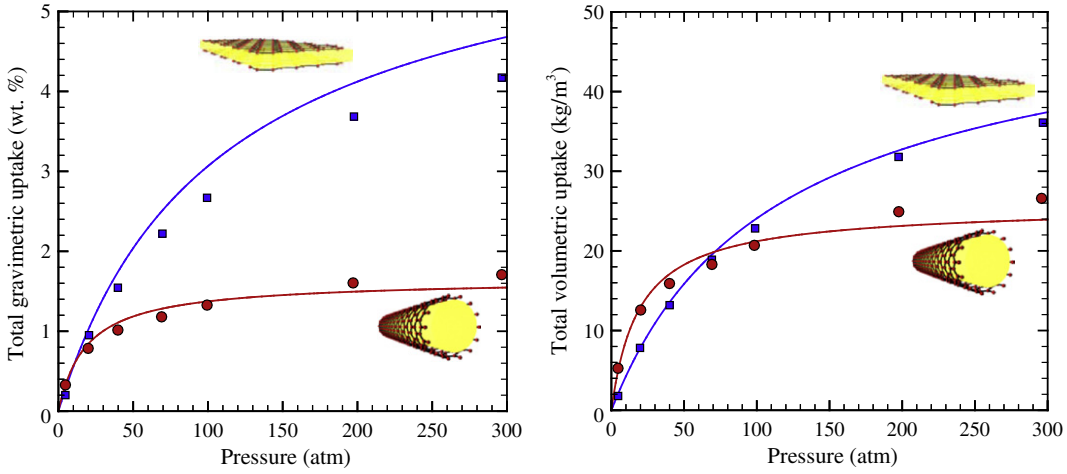

Fig. 3. TIMTAM prediction (solid lines) compared to simulation results for hydrogen gravimetric (left) and volumetric (right) uptakes within carbon slits (blue squares) and carbon nanotubes (red circles) of pore size 10 Å at different pressures and 200 K. Simulation data from Rzepka et al. [54]. (For interpretation of the references to color in this figure legend, the reader is referred to the web version of this article.)

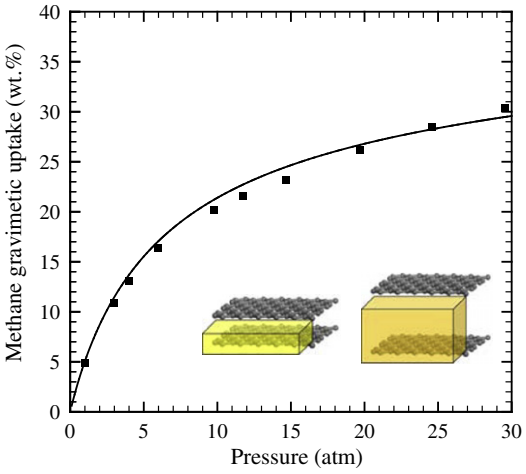

Fig. 4. TIMTAM prediction (solid line) compared to experimental methane uptake (squares) within activated carbon AX21 with average slit-shaped pore sizes of 12 and 21 Å with volume ratios of 45% and 65%, respectively. Data from Aukett et al. [61].

The TIMTAM model has also previously modeled hydrogen uptake successfully within IRMOF-8, -10 and -16, see Thornton et al. [11].

Finally, much interest has arisen in ZIFS, a new family of MOFs that provide a range of new topologies for carbon capture applications and other gas storage and separations [70]. These topologies can be represented as simple geometrical shapes, for example, SOD which we approximate as uniformed-sized spherical cavities, LTA which we approximate as two alternating spherical cavities and GME which we approximate as two cylindrical cavities, see Supplementary information. Similarly to the previous case for IRMOF-1, the potential energy within ZIFs is calculated by distributing the framework atoms continuously across the approximated cavity surface, as in Eq. (12). For ZIFs it is convenient to use the building blocks such as mIM, IM, nIM and cbIM, to make the calculation. For example, the structure of ZIF-8 (with SOD topology) is approximated as a series of spherical cavities (or cages) with 24 zinc atoms joined by 24 mIM bridging units making up its surface, hence with each mIM unit containing 2 nitrogen atoms, 4 carbon atoms and 6 hydrogen atoms, one can easily utilize Eq. (12) to predict the storage properties. This same approach was taken here for ZIF-69 with LTA topology and ZIF-76 with GME topology, where once again the cavity sizes were determined such that the actual free volume

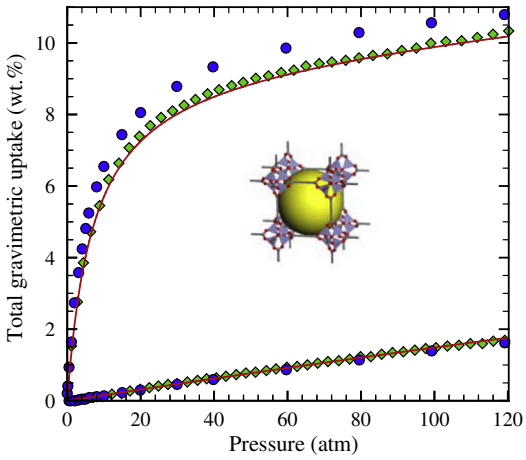

Fig. 5. TIMTAM prediction (solid red lines) for total hydrogen uptake to experimental results (green diamonds) and simulation results (blue circles) for IRMOF-1 at 77 (upper curve) and 298 (lower curve) K. Experimental data from Kaye et al. [63] and simulation data from Ryan et al. [62] Inset image of MOF geometry where yellow sphere closely resembles the TIMTAM cavity representation. (For interpretation of the references to color in this figure legend, the reader is referred to the web version of this article.)

matched that predicted by the approximated pore geometry. For consistency, the L-J parameter values established by Perez-Pellitero et al. are used here, see Table 1. As demonstrated in Fig. 6, the TIMTAM predictions for carbon dioxide uptakes match the experimental and simulation results reasonably well, which is quite remarkable considering that carbon dioxide is treated as a continuous medium where shape and dipole characteristics are not incorporated, and the internal structure is treated as a topological approximation.

The parameters ω and α were fitted for each family of structures because of their common morphology. Here we discuss the fundamental significance of these parameters and anticipate that these values will remain constant for future investigations within each family. As stated earlier, according to the theoretical composition of the model, both parameters play a role in representing the adsorbed phase, where ω represents the nature of the potential energy across the surface and α represents the adjusted heat loss (or heat remaining) upon adsorption. Practically, from the present use of the model, ω tends towards unity as the adsorption sites become more defined or specific, for example, MOFs and ZIFs have specific metal and ligand adsorption sites while nanotubes and graphene have non-specific continuous adsorption surfaces. Additionally, a larger α means that the heat loss during an adsorption event is inhibited by some energy-conserving feature, which could be adsorbate mobility or adsorbent flexibility. This is evident by the larger α values for carbon tubes and slits compared to MOFs and ZIFs, reflecting the fact that adsorbed molecules are more mobile across the "smoother" surfaces and more constricted on the surfaces with cornices. Either way, the results do not significantly

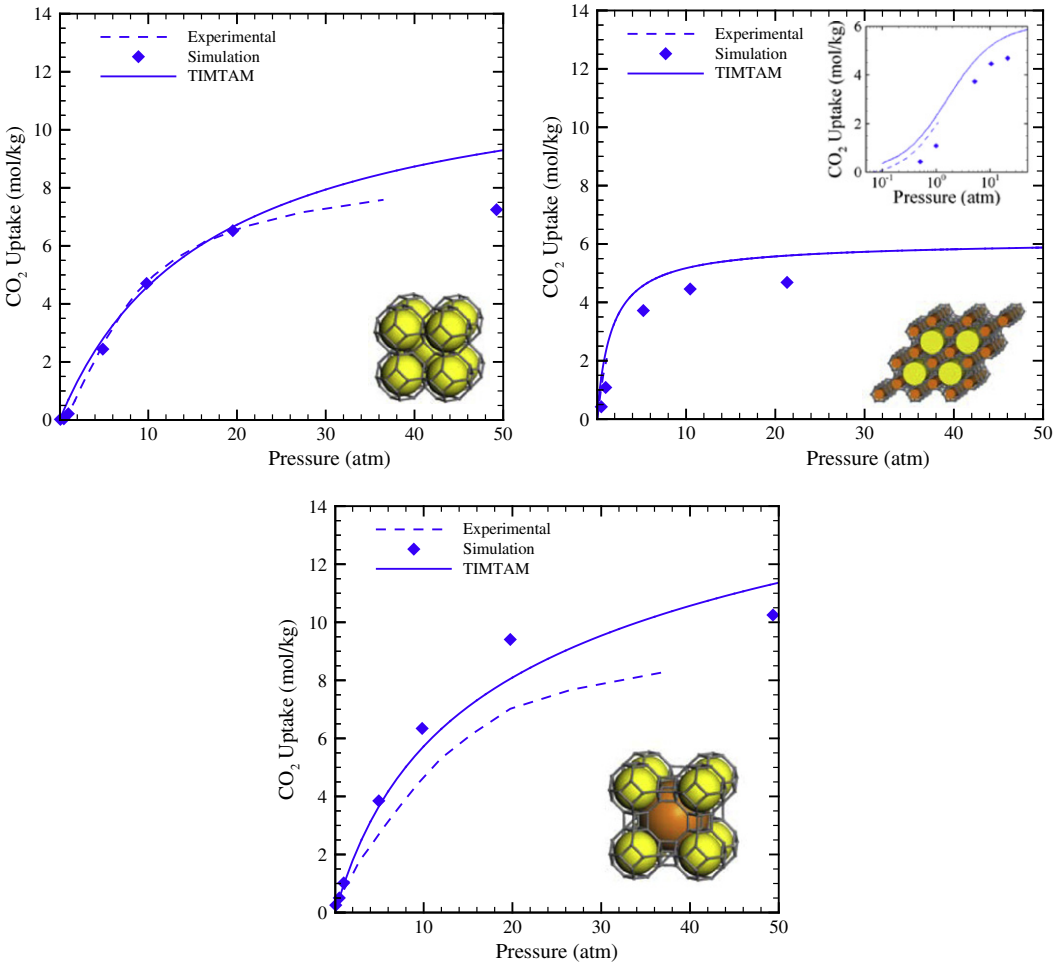

Fig. 6. Carbon dioxide uptake within (a) ZIF-8 (SOD topology), (b) ZIF-69 (GME topology) and (c) ZIF-76 (LTA topology). Experimental and simulation results from Perez-Pellitero et al. [64] versus TIMTAM predictions. Inset images of ZIF geometries where spheres and cylinders closely resemble the TIMTAM cavity representations.

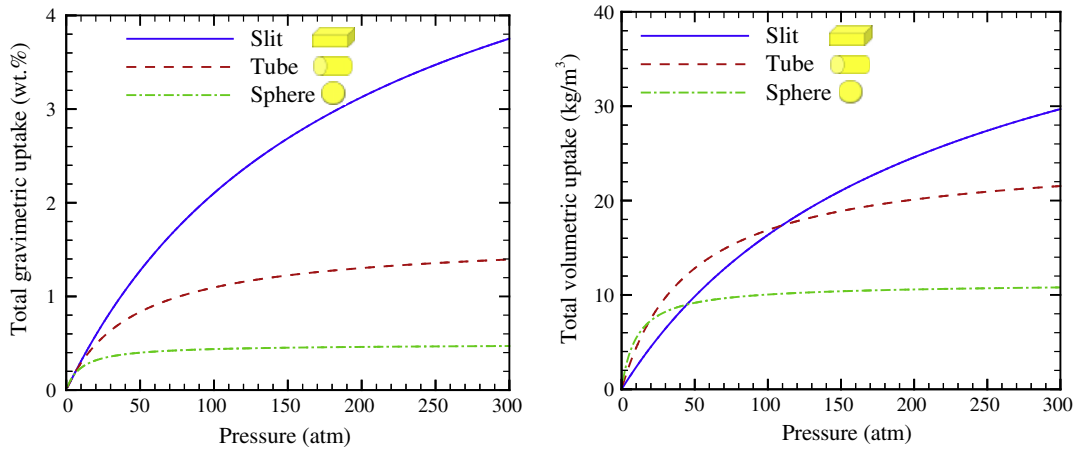

Fig. 7. TIMTAM results for total hydrogen gravimetric (left) and volumetric (right) uptake within carbon slits (blue), tubes (red) and spheres (green) with dimension 10 Å and at temperature 243 K. (For interpretation of the references to color in this figure legend, the reader is referred to the web version of this article.)

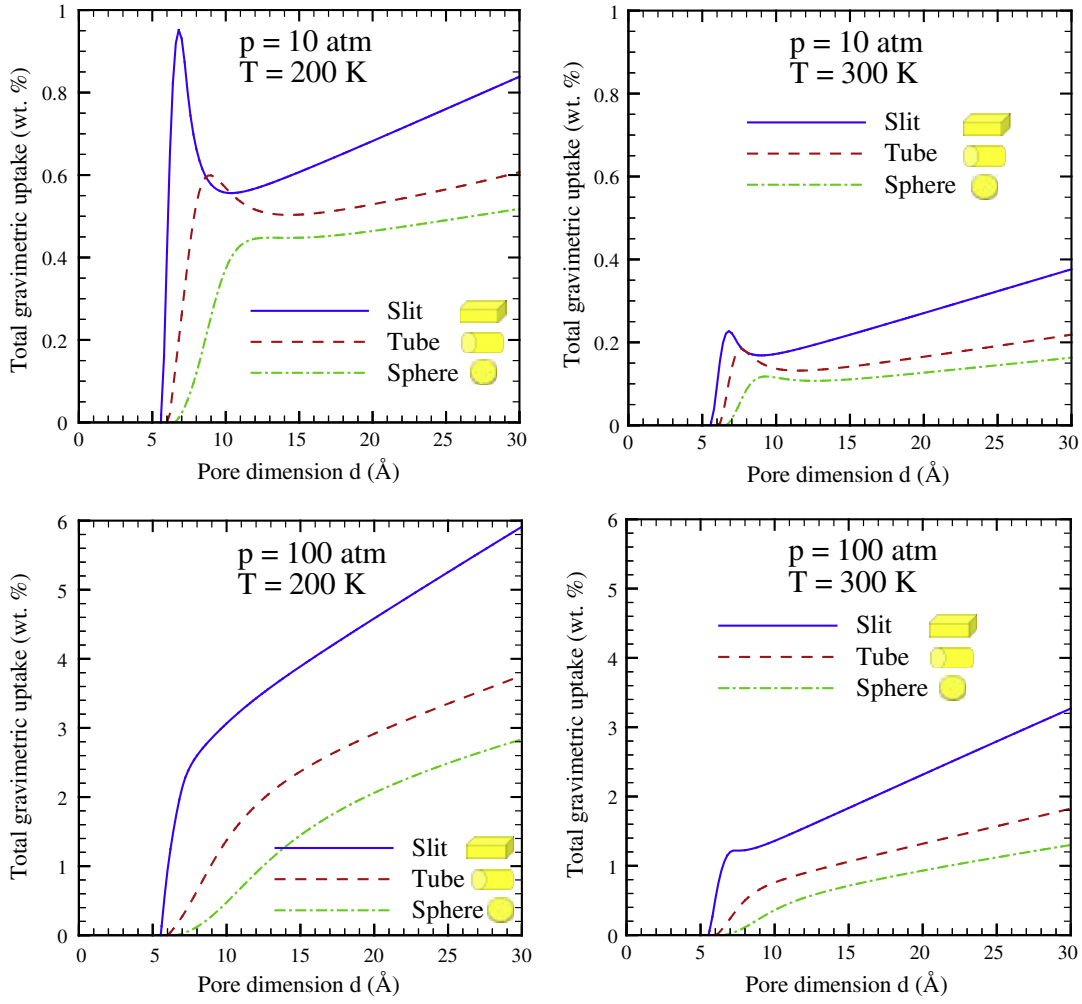

Fig. 8. TIMTAM results for total gravimetric hydrogen uptake within carbon slits (blue lines), tubes (red lines) and spheres (green lines) with varying pore sizes at four distinct combinations of pressures and temperatures. (For interpretation of the references to color in this figure legend, the reader is referred to the web version of this article.)

alter with varying ω or α, in fact, the saturation amount cannot be altered by these parameters which makes this final value more robust.

Here we have demonstrated success in predicting adsorption properties for H_2, CO_2 and CH_4 within various porous materials at various operating conditions; the predictions can be extended

predict adsorption for different gases, porosity, composition, conditions, etc.

An advantage of the TIMTAM approach is that it provides a fast way of exploring the range of values for the factors controlling adsorption. Pore size, free volume, system mass, heat of adsorption, temperature and pressure all play crucial roles in determining gas storage outcomes. Here we use TIMTAM to explore such factors.

Fig. 7 demonstrates the effect of pressure within carbon slits, tubes and spheres of dimension 10 Å and at temperature 243 K. The same parameter values used by Rzepka et al. [54] are used here. An important note is that the cavity shape with the highest uptake depends on the pressure, which means that the appropriate cavity shape can be selected according to the known operating pressure. This observation is more noticeable from the volumetric uptake. Frost et al. [68] provide an explanation for this in that at low pressures the heat of adsorption is the dominant factor while at higher pressures the free volume becomes the dominant factor. The heat of adsorption is greatest in spherical cavities and lowest in slit-shaped cavities, while free volume is greatest in slit-shaped cavities and lowest in spherical cavities. Therefore the observation is a result of the competition between the dominating factors, the heat of adsorption and free volume at various pressures.

As there are many possible combinations of temperature, pressure and pore size, Figs. 8 and 9 show the gravimetric and volumetric uptake within carbon slits, tubes and spheres of varying pore sizes at four distinct pressures and temperatures. Slit-shaped cavities outperform the other shaped cavities in gravimetric uptake due mainly to the higher volume to mass ratio (Fig. 8). However, the cavity shape delivering the highest volumetric uptake depends on cavity size, temperature and pressure (Fig. 9). At small pore sizes the gas uptake is restricted by the free volume available in each cavity shape. At large pore sizes the volumetric uptake tends toward that of compressed gas (no adsorbent); slit-shaped cavities approach this limit first followed by cylindrical cavities and spherical cavities. This is because the pore surfaces with higher curvature (higher heat of adsorption) cause denser adsorption layers to form along the surface which keeps the uptake higher than that of compressed gas until pores become larger where the influence of curvature decreases and the ratio of surface adsorption to bulk gas decreases.

Overall TIMTAM encompasses all the characteristics observed in gas adsorption phenomena: the amount of molecules in adsorbed and bulk gas phase increases with decreasing temperature and increasing pressure; the amount of molecules in the adsorbed phase increases with increasing heat of adsorption; heat of adsorption is proportional to the magnitude of potential energy for adsorption which increases with decreasing pore size, increasing surface curvature and increasing well depth of surface atoms; and finally, gravimetric uptake increases with decreasing surface mass.

We anticipate that this versatile approach will be applied to a wide range of porous materials including porous crystals such as zeolites and MOFs, carbon structures such as nanotubes, graphene and fullerenes, or even porous sedimentary rock for coal seam gas (or shale gas) exploration where quick estimates are useful. The potential downfalls of the approach will likely occur in scenarios

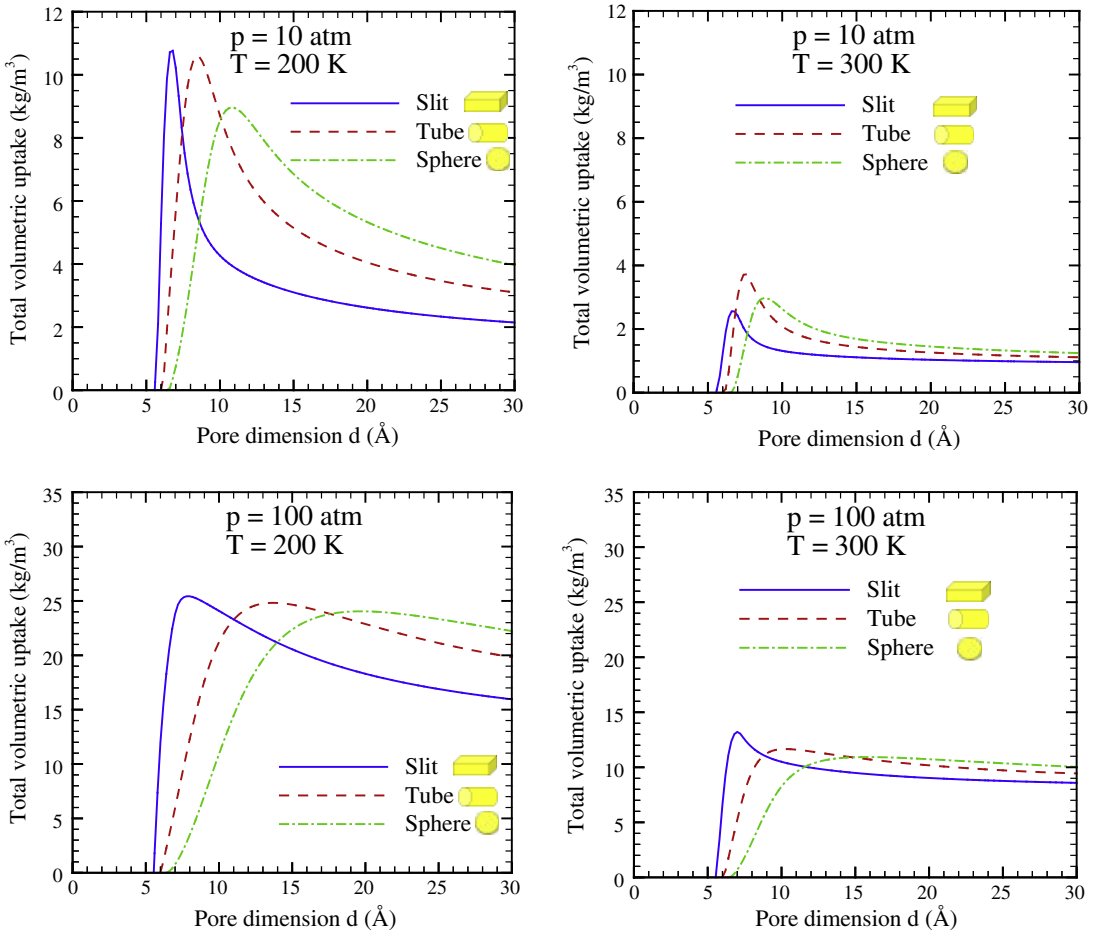

Fig. 9. TIMTAM results for total volumetric hydrogen uptake within carbon slits (blue lines), tubes (red lines) and spheres (green lines) with varying pore sizes at four distinct combinations of pressures and temperatures. (For interpretation of the references to color in this figure legend, the reader is referred to the web version of this article.)

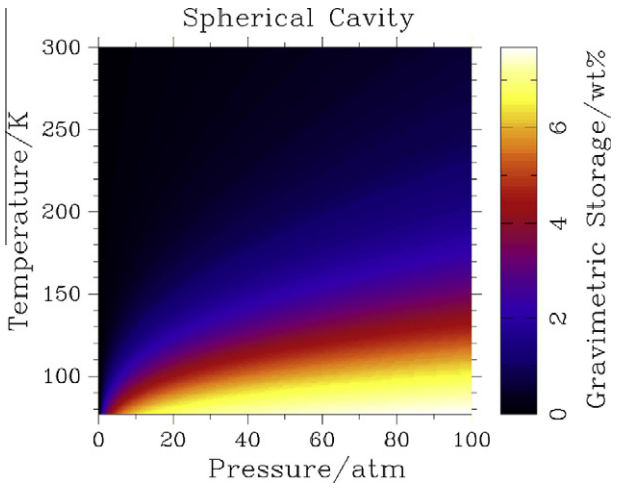

Fig. 10. Screen shot of Adsorb IT with 2D color plots generated by the TIMTAM routine for H_2 within IRMOF-1. See Table 1 for parameter values. Adsorb IT software available from corresponding author. (For interpretation of the references to color in this figure legend, the reader is referred to the web version of this article.)

where the specific atomic details of the material critically affect adsorption such as open metal sites or pores not captured in the pore size approximation. Additionally, the reliance on existing forcefields may cause the model to inaccurately model new materials with exotic elements such as the beryllium-based MOF [10]. Condensation or quantum effects are not captured in the current model. Surface or molecule polarity could be incorporated by utilizing an appropriate potential function such as the Morse potential, which is currently being formulated within our group.

Therefore, the TIMTAM approach is an excellent tool to guide material design for gas storage applications. A basic software package has been developed to implement the TIMTAM algorithm; examples for uptake within IRMOF-1 are shown in Fig. 10. The 2D color plots were generated within 30 s. This demonstrates the model's ability to speedily explore a large parameter space, a capability unachievable through statistical simulation techniques. Future work will focus on adding a built-in capability to automatically approximate complex structures into topologically simple shapes.

4. Conclusions

The TIMTAM formulation has been established to provide a simple method for predicting gas uptake capacities within a variety of porous materials for which the Langmuir or BET adsorption isotherms are inappropriate. Good agreement between experiment and simulation for uptake of H_2, CH_4 and CO_2 has been demonstrated, with variations typically less than 15%. The continuum-based model can be readily applied to cylindrical, spherical or slit-shaped pores. The model is able to account for the effects of temperature, pressure, adsorption enthalpy and pore topology on gas isotherms. TIMTAM is a method that can readily be used by those without extensive experience in modeling, and a graphical user interface for TIMTAM is available from the authors upon request. The model represents a significant step in accelerating materials discovery for important applications including storage media for gaseous fuels, clean energy applications, exploiting H_2 and CH_4, and for the capture of environmentally threatening gases such as CO_2.

Consequently the model has been applied to investigate the effects of pore size, free volume, heat of adsorption, system mass, pressure and temperature upon gas storage performance, highlighting the available parameter space for further development of gas storage media.

Acknowledgements

This work is partially supported by the Australian Research Council Discovery Project scheme. J.M.H. is grateful to the Australian Research Council for provision of an Australian Professorial Fellowship. A.W.T. gratefully acknowledges the CSIRO Division of Materials Science and Engineering and the OCE Science team. A.J.H. and M.R.H. thank the OCE Science Leader Scheme for funding.

Appendix A. Supplementary information

Supplementary information associated with this article can be found, in the online version, at http://dx.doi.org/10.1016/j.micromeso.2012.09.002.

References

[1] J. Baxter, Z. Bian, G. Chen, D. Danielson, M.S. Dresselhaus, A.G. Fedorov, T.S. Fisher, C.W. Jones, E. Maginn, U. Kortshagen, A. Manthiram, A. Nozik, D.R. Rolison, T. Sands, L. Shi, D. Sholl, Y. Wu, Energy Environ. Sci. 2 (2009) 559–588.
[2] M.Z. Jacobson, Energy Environ. Sci. 2 (2009) 148–173.
[3] D.M. D'Alessandro, B. Smit, J.R. Long, Angew. Chem. Int. Ed. 49 (2010) 6058–6082.
[4] C.A. Scholes, K.H. Smith, S.E. Kentish, G.W. Stevens, Int. J. Greenhouse Gas. Control 4 (2010) 739–755.
[5] J.M. Simmons, H. Wu, W. Zhou, T. Yildirim, Energy Environ. Sci. 4 (2011) 2177–2185.
[6] E.W. Wolff, Nature 470 (2011) 49–50.
[7] Multi-Year Research, Development and Demonstration Plan – Planned Program Activities for 2003–2010: Technical Plan. U.S. Department of Energy. Available from: <http://www.eere.energy.gov/hydrogenandfuelcells/mypp/pdfs/storage.pdf>.
[8] M. Eddaoudi, J. Kim, N. Rosi, D. Vodak, J. Wachter, M. O'Keeffe, O.M. Yaghi, Science 295 (2002) 469–472.
[9] J.L.C. Rowsell, O.M. Yaghi, Micropor. Mesopor. Mater. 73 (2004) 3–14.
[10] K. Sumida, M.R. Hill, S. Horike, A. Dailly, J.R. Long, J. Am. Chem. Soc. 131 (2009) 15120–15121.
[11] A.W. Thornton, K.M. Nairn, J.M. Hill, A.J. Hill, M.R. Hill, J. Am. Chem. Soc. 131 (2009) 10662–10669.
[12] K.S. Park, Z. Ni, A.P. Cote, J.Y. Choi, R. Huang, F.J. Uribe-Romo, H.K. Chae, M. O'Keeffe, O.M. Yaghi, Proc. Natl. Acad. Sci. USA 103 (2006) 10186–10191.
[13] R. Banerjee, A. Phan, B. Wang, C. Knobler, H. Furukawa, M. O'Keeffe, O.M. Yaghi, Science 319 (2008) 939–943.
[14] W. Morris, C.J. Doonan, H. Furukawa, R. Banerjee, O.M. Yaghi, J. Am. Chem. Soc. 130 (2008) 12626–12627.
[15] A.C. Dillon, K.M. Jones, T.A. Bekkedahl, C.H. Kiang, D.S. Bethune, M.J. Heben, Nature 386 (1997) 377–379.
[16] F. Darkrim, D. Levesque, J. Chem. Phys. 109 (1998) 4981–4984.
[17] C. Liu, Y.Y. Fan, M. Liu, H.T. Cong, H.M. Cheng, M.S. Dresselhaus, Science 286 (1999) 1127–1129.
[18] Q. Wang, J.K. Johnson, J. Chem. Phys. 110 (1999) 577–586.
[19] S.K. Bhatia, A.L. Myers, Langmuir 22 (2006) 1688–1700.
[20] A. Gigras, S.K. Bhatia, A.V.A. Kumar, A.L. Myers, Carbon 45 (2007) 1043–1050.
[21] T. Ben, C. Pei, D. Zhang, J. Xu, F. Deng, X. Jing, S. Qiu, Energy Environ. Sci. 4 (2011) 3991–3999.
[22] N. Alam, R. Mokaya, Energy Environ. Sci. 3 (2011) 1773–1781.
[23] I. Langmuir, J. Am. Chem. Soc. 38 (1916) 2221–2295.
[24] S. Brunauer, P.H. Emmett, E. Teller, J. Am. Chem. Soc. 60 (1938) 309–319.
[25] A.I. Skoulidas, D.S. Sholl, J. Phys. Chem. B 109 (2005) 15760–15768.
[26] E. Pantatosaki, F.G. Pazzona, G. Megariotis, G.K. Papadopoulos, J. Phys. Chem. B 114 (2010) 2493–2503.
[27] D. Dubbeldam, R. Krishna, R.Q. Snurr, J. Phys. Chem. C 113 (2009) 19317–19327.
[28] A.I. Skoulidas, D.S. Sholl, J. Phys. Chem. A 107 (2003) 10132–10141.
[29] Z. Xiang, D. Cao, J. Lan, W. Wang, D.P. Broom, Energy Environ. Sci. 3 (2010) 1469–1487.
[30] S. Keskin, D.S. Sholl, Energy Environ. Sci. 3 (2010) 343–351.
[31] E. Beerdsen, D. Dubbeldam, B. Smit, Phys. Rev. Lett. 95 (2005) 164505.
[32] R.Q. Snurr, A.T. Bell, D.N. Theodorou, J. Phys. Chem. 97 (1993) 13742–13752.
[33] G. Garberoglio, Langmuir 23 (2007) 12154–12158.
[34] R. Babarao, Z.Q. Hu, J.W. Jiang, S. Chempath, S.I. Sandler, Langmuir 23 (2007) 659–666.
[35] T. Mueller, G. Ceder, J. Phys. Chem. B 109 (2005) 17974–17983.
[36] A.K. Rappe, C.J. Casewit, K.S. Colwell, W.A. Goddard, W.M. Skiff, J. Am. Chem. Soc. 114 (1992) 10024–10035.

[37] S.S. Han, J.L. Mendoza-Cortes, W.A. Goddard III, Soc. Rev. 38 (2009) 1460–1476.
[38] P. Dalach, H. Frost, R.Q. Snurr, D.E. Ellis, J. Phys. Chem. C 112 (2008) 9278–9284.
[39] E.A. Ustinov, Langmuir 25 (2009) 7450–7456.
[40] X. Zhang, D. Cao, J. Chen, J. Phys. Chem. B 107 (2003) 4942–4950.
[41] J. Lan, D. Cao, W. Wang, Langmuir 26 (2010) 220–226.
[42] E. Kierlik, P.A. Monson, M.L. Rosinberg, L. Sarkisov, G. Tarjus, Phys. Rev. Lett. 87 (2001) 055701.
[43] B.K. Peterson, K.E. Gubbins, Mol. Phys. 62 (1987) 215–226.
[44] T.C. Merkel, H. Lin, X. Wei, R. Baker, J. Membr. Sci. 359 (2010) 126–139.
[45] A. Gupta, S. Chempath, M.J. Sanborn, L.A. Clark, R.Q. Snurr, Mol. Simul. 29 (2003) 29–46.
[46] F.T. Willmore, X. Wang, I.C. Sanchez, J. Polym. Sci., Part B: Polym. Phys. 44 (2006) 1385–1393.
[47] D. Dubbeldam, S. Calero, D.E. Ellis, R.Q. Snurr, RASPA 1.0, Northwestern University, Evanston, 2008.
[48] A. Gupta, M.J. Sanborn, L.A. Clark, S. Chempath, L. Sarkisov, R.Q. Snurr, MUlti SImulation Code (MUSIC), Northwestern University, Evanston, IL, 2002.
[49] B.J. Cox, N. Thamwattana, J.M. Hill, J. Phys. A: Math. Theor. 41 (2008) 235209.
[50] T.A. Hilder, J.M. Hill, J. Phys. A: Math. Theor. 40 (2007) 3851–3868.
[51] P.W. Atkins, Physical Chemistry, Oxford University Press, Oxford, 1978.
[52] A.L. Myers, Int. Adsorpt. Soc. 9 (2003) 9–16.
[53] R.J. Sadus, J. Chem. Phys. 115 (2001) 1460–1462.
[54] M. Rzepka, P. Lamp, M. Casa-Lillo, J. Phys. Chem. B 102 (1998) 10894–10898.
[55] A.L. Myers, Thermodynamics of adsorption, in: T.M. Letcher (Ed.), Chemical Thermodynamics for Industry, Royal Society of Chemistry, Cambridge, 2004.
[56] C. Dieterici, Ann. Phys. Chem. Wiedemanns Ann. 69 (1899) 666–685.
[57] B. Panella, M. Hirscher, H. Putter, U. Muller, Adv. Funct. Mater. 16 (2006) 520–524.
[58] D. Farrusseng, C. Daniel, C. Gaudillere, U. Ravon, Y. Schuurman, C. Mirodatos, D. Dubbeldam, H. Frost, R.Q. Snurr, Langmuir 25 (2009) 7383–7388.
[59] D.H. Everett, J.C. Powl, Faraday Trans. 1 (72) (1976) 619–636.
[60] H. Furukawa, M. Miller, O.M. Yaghi, J. Mater. Chem. 17 (2007) 3197–3204.
[61] P.N. Aukett, N. Quirke, S. Riddiford, S.R. Tennison, Carbon 30 (1992) 913–924.
[62] P. Ryan, L.J. Broadbelt, R.Q. Snurr, Chem. Commun. (2008) 4132–4134.
[63] S.S. Kaye, A. Dailly, O.M. Yaghi, J.R. Long, J. Am. Chem. Soc. 129 (2007) 14176–14177.
[64] J. Pérez-Pellitero, H. Amrouche, F.R. Siperstein, G. Pirngruber, C. Nieto-Draghi, G. Chaplais, A. Simon-Masseron, D. Bazer-Bachi, D. Peralta, N. Bats, Chem. Eur. J. 16 (2010) 1560–1571.
[65] Maple, 10.00; Maplesoft, 2005.
[66] S.A. Furman, A.W. Thornton, Adsorb IT, 1.0; CSIRO, 2011.
[67] S.L. Mayo, B.D. Olafson, W.A. Goddard III, J. Phys. Chem. 94 (1990) 8897–8909.
[68] H. Frost, T. Duren, R.Q. Snurr, J. Phys. Chem. B 110 (2006) 9565–9570.
[69] L.F. Herrera, C. Fan, V. Nguyen, D.D. Do, T. Horikawa, D. Nocholson, Carbon 50 (2012) 500–509.
[70] A.W. Thornton, D. Dubbeldam, M.S. Liu, B.P. Ladewig, A.J. Hill, M.R. Hill, Energy Environ. Sci. 5 (2012) 7637–7646.